



High-Throughput Synthesis of Zeolitic Imidazolate Frameworks and Application to CO₂ Capture

Rahul Banerjee, *et al.*
Science **319**, 939 (2008);
DOI: 10.1126/science.1152516

The following resources related to this article are available online at www.sciencemag.org (this information is current as of February 15, 2008):

Updated information and services, including high-resolution figures, can be found in the online version of this article at:

<http://www.sciencemag.org/cgi/content/full/319/5865/939>

Supporting Online Material can be found at:

<http://www.sciencemag.org/cgi/content/full/319/5865/939/DC1>

A list of selected additional articles on the Science Web sites **related to this article** can be found at:

<http://www.sciencemag.org/cgi/content/full/319/5865/939#related-content>

This article **cites 19 articles**, 1 of which can be accessed for free:

<http://www.sciencemag.org/cgi/content/full/319/5865/939#otherarticles>

This article appears in the following **subject collections**:

Chemistry

<http://www.sciencemag.org/cgi/collection/chemistry>

Information about obtaining **reprints** of this article or about obtaining **permission to reproduce this article** in whole or in part can be found at:

<http://www.sciencemag.org/about/permissions.dtl>

NH₃/HCl and ND₃/DCl mixtures condensed in an argon matrix have been reported (28). Their spectra yield ($\nu = 0 \rightarrow 1$) vibrational transition values of 1371 and 1113 cm⁻¹, respectively, for the N...H/D...Cl stretching modes of the proton-transferred species, NH₄⁺Cl⁻ and ND₄⁺Cl⁻. Because our spacings are extracted from highly anharmonic parts of the progressions and the (0 \rightarrow 1) vibrational frequencies are strongly affected by matrix effects (28, 29), the agreement is satisfactory. The first three calculated spacings between the energy levels associated with various excitations of the central hydrogen atom are 1718 (0 to 1), 1171 (1 to 2), and 1214 (2 to 3) cm⁻¹. The latter value of 1214 cm⁻¹ matches very well the spacing between the two most prominent peaks [1218 cm⁻¹ (0.151 eV)], suggesting that the two strongest peaks in the (NH₄⁺Cl⁻)⁻ spectrum can be assigned as transitions from $\nu'' = 0$ in the anionic complex to $\nu' = 2$ and 3, respectively, in the neutral manifold (ν'' denotes vibrational quantum numbers in the anion, ν' signifies those in the neutral).

The secondary vibrational structure in the photoelectron spectra is likely associated with low-frequency vibrational modes, a prime candidate being the Cl-N intermolecular stretching mode. This is supported by the calculated decrease of the Cl-N distance by 0.249 Å from the neutral to the anion (Fig. 3). Both for the neutral and the anion, the theoretical calculations showed strong coupling between the central hydrogen and intermolecular stretching modes. (These two modes are schematically depicted in Fig. 2.) We calculated anharmonic spacings in the 155 to 172 cm⁻¹ range (~0.02 eV) for the first five energy levels of the intermolecular stretching mode in the neutral complex.

These intermolecular stretching progressions are similar to those seen by Lineberger and co-workers (30) in their seminal work measuring the photoelectron spectra of the alkali halide anions. There are clear similarities between the current system, NH₄⁰Cl⁻, and the alkali halide anions, (MX)⁻, which have also been described as M⁰X⁻. Their spectra, however, are dominated by the only available degree of freedom, the M-X stretch, whereas in the ammonia-hydrogen chloride system, transitions from that mode are far less prominent, with the N...H/D...Cl stretch giving rise to the dominant transitions.

References and Notes

- R. S. Mulliken, W. B. Person, *Molecular Complexes, A Lecture and Reprint Volume* (Wiley-Interscience, New York, 1969).
- N. W. Howard, A. C. Legon, *J. Chem. Phys.* **88**, 4694 (1988).
- A. C. Legon, *Chem. Soc. Rev.* **22**, 153 (1993).
- B. Cherng, F.-M. Tao, *J. Chem. Phys.* **114**, 1720 (2001).
- F.-M. Tao, *J. Chem. Phys.* **110**, 11121 (1999).
- R. Cazar, A. Jamka, F.-M. Tao, *Chem. Phys. Lett.* **287**, 549 (1998).
- I. Alkorta, I. Rozas, O. Mo, M. Yanez, J. Elguero, *J. Phys. Chem. A* **105**, 7481 (2001).
- A. Brčić, A. Karpfen, H. Lischka, P. Schuster, *Chem. Phys.* **89**, 337 (1984).

- A. Famulari, M. Sironi, M. Raimondi, in *Quantum Systems in Chemistry and Physics* (Springer, Netherlands, 2000), vol. 1, pp. 361–379.
- Z. Latajka, S. Sakai, K. Morokuma, H. Ratajczak, *Chem. Phys. Lett.* **110**, 464 (1984).
- G. Corongiu *et al.*, *Int. J. Quant. Chem.* **59**, 119 (1996).
- S. Y. Reece, J. M. Hodgkiss, J. Stubbe, D. G. Nocera, *Philos. Trans. R. Soc. B* **361**, 1351 (2006).
- D. Radisic *et al.*, *J. Am. Chem. Soc.* **127**, 6443 (2005).
- J.-Y. Fang, S. Hammes-Schiffer, *J. Chem. Phys.* **106**, 8442 (1997).
- J. V. Coe, J. T. Snodgrass, C. B. Friedhoff, K. M. McHugh, K. H. Bowen, *J. Chem. Phys.* **87**, 4302 (1987).
- MOLPRO, version 2006.1, a package of ab initio programs; H. J. Werner *et al.* (www.molpro.net).
- Gaussian 03, Revision C.02; M. J. Frisch *et al.*, Gaussian, Inc., Wallingford CT, 2004.
- P. R. Taylor, *Lecture Notes in Quantum Chemistry II*, B. O. Roos, Ed. (Springer-Verlag, Berlin, 1994).
- We used augmented, polarized, correlation consistent basis sets of double- and triple-zeta quality (31) supplemented with additional diffuse s and p functions centered on the nitrogen atom with exponents chosen to describe the excess electron-charge distribution in the dipole-bound anion (ClH⁻NH₃)⁻.
- B. C. Garrett, D. G. Truhlar, *J. Am. Chem. Soc.* **101**, 5207 (1979).
- D. T. Colbert, W. H. Miller, *J. Chem. Phys.* **96**, 1982 (1992).
- C. S. Brauer *et al.*, *J. Phys. Chem. A* **110**, 10025 (2006).
- C. Desfrancois *et al.*, *Phys. Rev. Lett.* **72**, 48 (1994).
- R. N. Compton *et al.*, *J. Chem. Phys.* **105**, 3472 (1996).
- P. Skurski, M. Gutowski, *J. Chem. Phys.* **111**, 3004 (1999).
- G. Herzberg, *Annu. Rev. Phys. Chem.* **38**, 27 (1987).
- R. A. Bachorz, M. Haranczyk, I. Dabowska, J. Rak, M. Gutowski, *J. Chem. Phys.* **122**, 204304 (2005).
- A. J. Barnes, T. R. Beech, Z. Mielke, *J. Chem. Soc. Faraday Trans. II* **80**, 455 (1984).
- M. J. T. Jordan, J. E. Del Bene, *J. Am. Chem. Soc.* **122**, 2101 (2000).
- T. M. Miller, D. G. Leopold, K. K. Murray, W. C. Lineberger, *J. Chem. Phys.* **85**, 2368 (1986).
- R. A. Kendall, T. H. Dunning Jr., R. J. Harrison, *J. Chem. Phys.* **96**, 6796 (1992).
- ChemCraft Version 1.5 (build 276), www.chemcraftprog.org.
- This material is based in part on work supported by National Science Foundation grant CHE-0517337 (K.H.B.). We also thank the Polish State Committee for Scientific Research (KBN) for support under grants DS/8000-4-0026-8 (M.G.) and N204 127 31/2963 (M.H.) and the U.S. Department of Energy (DOE) Office of Basic Energy Sciences Chemical Sciences program (M.G. and G.K.S.). The research of R.A.B. was supported by the Deutsche Forschungsgemeinschaft (DFG) through the Center for Functional Nanostructures (CFN, Project No. C3.3) and by a grant from the Ministry of Science, Research and the Arts of Baden-Württemberg (Az: 7713.14-300). M.H. is a holder of an award from the Foundation for Polish Science (FNP). This research was performed in part at the Molecular Science Computing Facility in the William R. Wiley Environmental Molecular Sciences Laboratory at Pacific Northwest National Laboratory, operated for the U.S. DOE by Battelle.

Supporting Online Material

www.sciencemag.org/cgi/content/full/319/5865/936/DC1
Table S1

11 October 2007; accepted 21 December 2007
10.1126/science.1151614

High-Throughput Synthesis of Zeolitic Imidazolate Frameworks and Application to CO₂ Capture

Rahul Banerjee,^{1*} Anh Phan,¹ Bo Wang,¹ Carolyn Knobler,¹ Hiroyasu Furukawa,¹ Michael O'Keeffe,² Omar M. Yaghi^{1*}

A high-throughput protocol was developed for the synthesis of zeolitic imidazolate frameworks (ZIFs). Twenty-five different ZIF crystals were synthesized from only 9600 microreactions of either zinc(II)/cobalt(II) and imidazolate/imidazolate-type linkers. All of the ZIF structures have tetrahedral frameworks: 10 of which have two different links (heterolinks), 16 of which are previously unobserved compositions and structures, and 5 of which have topologies as yet unobserved in zeolites. Members of a selection of these ZIFs (termed ZIF-68, ZIF-69, and ZIF-70) have high thermal stability (up to 390°C) and chemical stability in refluxing organic and aqueous media. Their frameworks have high porosity (with surface areas up to 1970 square meters per gram), and they exhibit unusual selectivity for CO₂ capture from CO₂/CO mixtures and extraordinary capacity for storing CO₂: 1 liter of ZIF-69 can hold ~83 liters of CO₂ at 273 kelvin under ambient pressure.

High-throughput methods are routinely used in screening for activity of drug molecules and catalysts, but their use in the synthesis of new crystalline solid-state compounds remains relatively undeveloped. Often, the products are either known compounds or ones with condensed extended structures (1–7). For multicomponent chemical systems, such as in the synthesis of porous metal-organic structures, it would be reasonable to assume that the most energetically favored structures

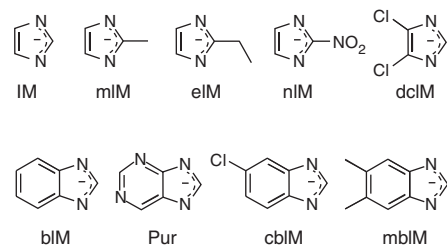
would result and that these would be known structures and topologies. Another challenge in solid-state synthesis is overcoming the propen-

¹Center for Reticular Chemistry at California NanoSystems Institute, Department of Chemistry and Biochemistry, University of California at Los Angeles, 607 East Charles E. Young Drive, Los Angeles, CA 90095, USA. ²Department of Chemistry and Biochemistry, Arizona State University, Tempe, AZ 85287, USA.

*To whom correspondence should be addressed. E-mail: rahul@chem.ucla.edu (R.B.); yaghi@chem.ucla.edu (O.M.Y.)

sity for producing multiple phases when mixed linkers are used in the synthesis (i.e., several phases each containing one kind of linker, rather than one phase containing mixed “hetero” linkers).

We show that high-throughput methods can be successfully applied to developing a robust synthesis protocol for ZIFs. Not only does this approach consistently yield only tetrahedral porous ZIF structures, but it also allows access to ZIF topologies previously un-



Scheme 1.

realized in ZIFs or in other zeolite materials. We also show that ZIFs with heterolinks can be produced that provide a greater level of complexity into the pore composition and structure, thus impacting the selectivity and multifunctionality of the pores. Specifically, the high-throughput syntheses and structures of 25 ZIFs are described and studied. All are open tetrahedral structures: 10 have heterolinks, 16 are previously unreported compositions and structures, and 5 have topologies heretofore unobserved in zeolite science. Among them are ZIFs with large (>10 Å) aperture pores, which opens up possibilities for application of these materials. We show that their synthesis is scalable to multigram quantities, using the same conditions used in the high-throughput method, and that the frameworks have extraordinary thermal and chemical stability, as well as high porosity. We find that several ZIFs with heterolinks have pores that can affect exceptional selective capture and storage of CO_2 .

We (8, 9) and others (10–14) have recently reported the synthesis of ZIFs in which (i) transition metal atoms (M, specifically Zn and Co) replace T atoms (tetrahedral linkers such as Si, Al, and P) and (ii) imidazolates (IMs) (Scheme 1) replace bridging oxides in zeolites. Given that the M–IM–M angle is near 145° and that it is coincident with the Si–O–Si angle preferred and commonly found in many zeolites, we were hopeful that the class of ZIF materials would at least be as extensive as that of zeolites (15, 16). We set out to develop the ZIF portfolio and quickly found that the traditional synthesis used to discover the original ZIFs was tedious, unpredictable, and time consuming, and that it required wastefully large amounts of solvents and reagents (8, 9). We targeted, among other goals, structures with heterolinks (Scheme 1) based on a wide variety of available IM units and studied their application to the selective capture of CO_2 .

The general ZIF reaction examined is composed of one or two of these nine different

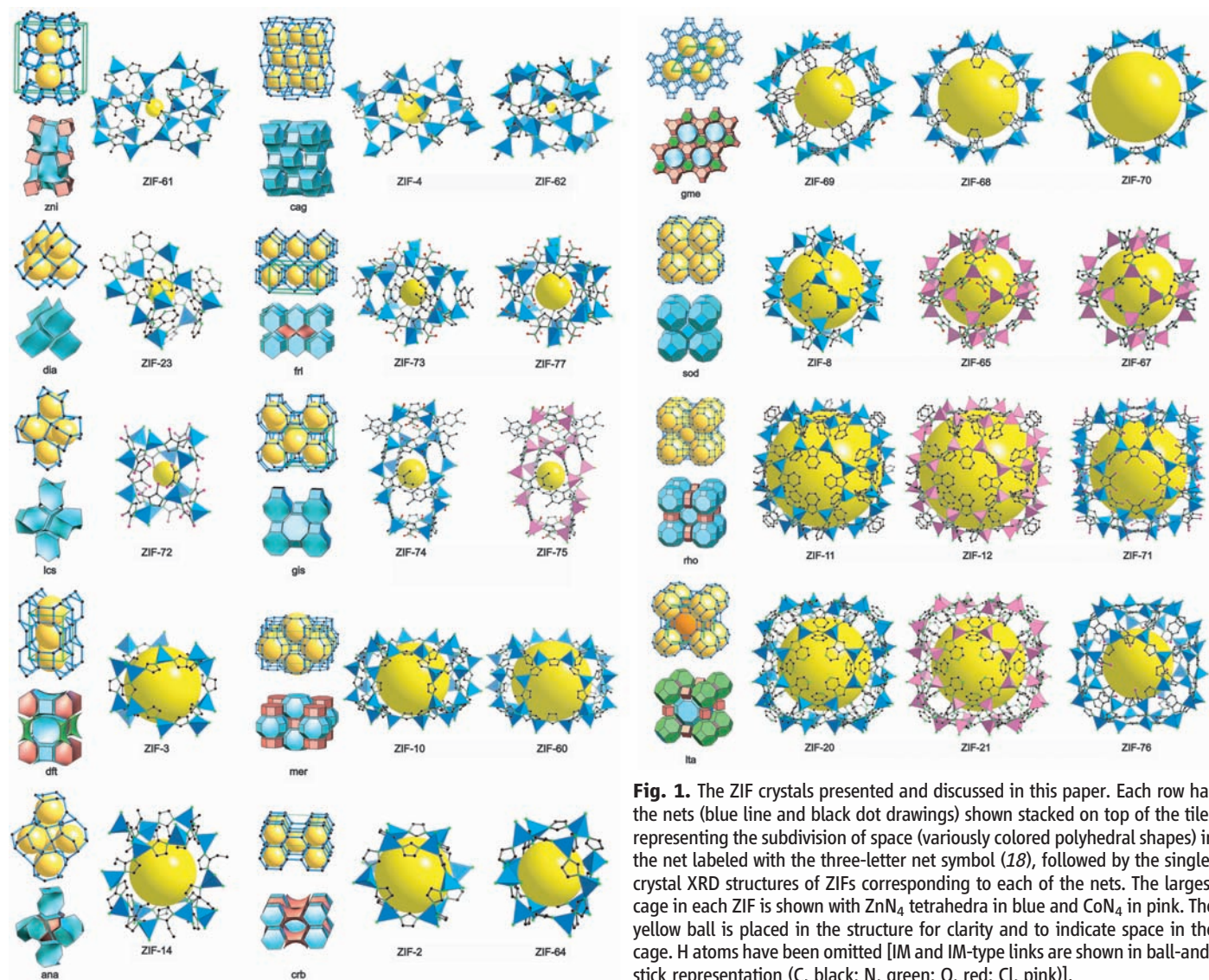


Fig. 1. The ZIF crystals presented and discussed in this paper. Each row has the nets (blue line and black dot drawings) shown stacked on top of the tiles representing the subdivision of space (variously colored polyhedral shapes) in the net labeled with the three-letter net symbol (18), followed by the single-crystal XRD structures of ZIFs corresponding to each of the nets. The largest cage in each ZIF is shown with ZnN_4 tetrahedra in blue and CoN_4 in pink. The yellow ball is placed in the structure for clarity and to indicate space in the cage. H atoms have been omitted [IM and IM-type links are shown in ball-and-stick representation (C, black; N, green; O, red; Cl, pink)].

IM-type links, which were reacted with either zinc(II) nitrate or cobalt(II) nitrate in *N,N'*-dimethylformamide or *N,N'*-diethylformamide. In total, we used 100 plates (9600 wells, 0.30 ml reactant volume per well) [supporting online material (SOM) text S1]. The metal-to-linker mole ratio was varied from 1:1 to 1:12. These amounts were dispensed with an automated dispensing unit charged with a stock solution whose concentration was also varied from 0.075 to 0.20 M for both reactants. After loading the mixture of reactants into the wells, the plates were covered with a polytetrafluoroethylene sheet, sealed, and then heated to a temperature range of 65° to 150°C for 48 to 100 hours. Crystalline products of ZIFs were obtained in this temperature range. Photographic images of wells containing crystals (0.1 to 1.0 mm) are shown in SOM text S2. After a preliminary analysis by automated powder x-ray diffraction (PXRD) (17), crystals for single-crystal x-ray diffraction (XRD) studies were then selected from those wells containing new materials (SOM text S2). In general, we found that a concentration level of 0.20 M, a reaction time of 72 hours, and an isothermal temperature of 85° or 100°C were optimal for ZIF synthesis and crystallization.

We isolated 25 different crystals using this protocol for single-crystal structural characterization (Table 1, Fig. 1, and SOM text S2). Among the 25 crystal structures, 9 are based on ZIFs already discovered by the traditional method (ZIF-2 to ZIF-23) (8, 9), whereas 16 have a new composition

Table 1. The ZIFs discovered by high-throughput synthesis. Dashes indicate no zeolite symbol.

ZIF- <i>n</i>	Composition	Net (18)	Zeolite (15)	<i>T/V</i> (nm ⁻³)	<i>d_a</i> (Å)	<i>d_p</i> (Å)	<i>N</i> †	Transitivity	Cage
2	Zn(IM) ₂	crb	BCT	2.80	6.4	6.9	12	1232	[6 ² .8 ²]
3*	Zn(IM) ₂	dft	DFT	2.66	4.6	6.0	16	1353	[6 ² .8 ⁴]
4	Zn(IM) ₂	cag	-	2.04	2.0	2.1	20	1431	[4 ² .6 ⁸]
8	Zn(mIM) ₂	sod	SOD	2.47	3.4	11.6	24	1121	[4 ⁶ .6 ⁸]
10	Zn(IM) ₂	mer	MER	2.25	8.2	12.1	24	1463	[4 ¹² .8 ⁶]
11	Zn(bIM) ₂	rho	RHO	2.01	3.0	14.6	48	1242	[4 ¹² .6 ⁸ .8 ⁶]
12	Co(bIM) ₂	rho	RHO	2.01	3.0	14.6	48	1242	[4 ¹² .6 ⁸ .8 ⁶]
14	Zn(eIM) ₂	ana	ANA	2.47	2.2	2.2	24	1132	[6 ² .8 ³]
20	Zn(Pur) ₂	lta	LTA	2.04	2.8	15.4	48	1343	[4 ¹² .6 ⁸ .8 ⁶]
21	Co(Pur) ₂	lta	LTA	2.03	2.8	15.4	48	1343	[4 ¹² .6 ⁸ .8 ⁶]
23*	Zn(abIM) ₂	dia	-	3.31	1.1	4.2	10	1111	[6 ⁴]
60	Zn(IM) _{1.5} (mIM) _{0.5}	mer	MER	2.24	7.2	9.4	24	1463	[4 ¹² .8 ⁶]
61	Zn(IM)(mIM)	zni	-	4.62	0.7	0.7	20	1342	[6 ³ .12 ²]
62	Zn(IM) _{1.75} (bIM) _{0.25}	cag	-	3.52	1.4	1.3	20	1431	[4 ² .6 ⁸]
64	Zn(IM) ₂	crb	BCT	3.62	2.5	7.9	12	1232	[6 ² .8 ²]
65	Co(nIM) ₂	sod	SOD	2.32	3.4	10.4	24	1121	[4 ⁶ .6 ⁸]
67	Co(mIM) ₂	sod	SOD	2.46	3.4	11.6	24	1121	[4 ⁶ .6 ⁸]
68	Zn(bIM)(nIM)	gme	GME	2.12	7.5	10.3	24	1463	[4 ⁶ .8 ³ .12 ²]
69	Zn(cbIM)(nIM)	gme	GME	2.09	4.4	7.8	24	1463	[4 ⁶ .8 ³ .12 ²]
70	Zn(lm) _{1.13} (nIM) _{0.87}	gme	GME	2.10	13.1	15.9	24	1463	[4 ⁶ .8 ³ .12 ²]
71	Zn(dclIM) ₂	rho	RHO	2.06	4.2	16.5	48	1242	[4 ¹² .6 ⁸ .8 ⁶]
72	Zn(dclIM) ₂	lcs	-	3.16	1.9	1.9	12	1121	[6 ⁵]
73	Zn(nIM) _{1.74} (mbIM) _{0.26}	frl	-	3.20	1.0	1.0	16	2342	[4 ⁴ .6 ² .8 ²]
74	Zn(nIM)(mbIM)	gis	GIS	2.66	1.2	2.6	20	1231	[4 ⁶ .8 ⁴]
75	Co(nIM)(mbIM)	gis	GIS	2.66	1.2	2.62	20	1231	[4 ⁶ .8 ⁴]
76	Zn(IM)(cbIM)	lta	LTA	2.05	5.4	12.2	48	1343	[4 ¹² .6 ⁸ .8 ⁶]
77	Zn(nIM)	frl	-	3.22	2.9	3.6	16	2342	[4 ⁴ .6 ² .8 ²]

*Discovered by traditional synthesis methods. †*N* is the number of vertices of the largest cage.

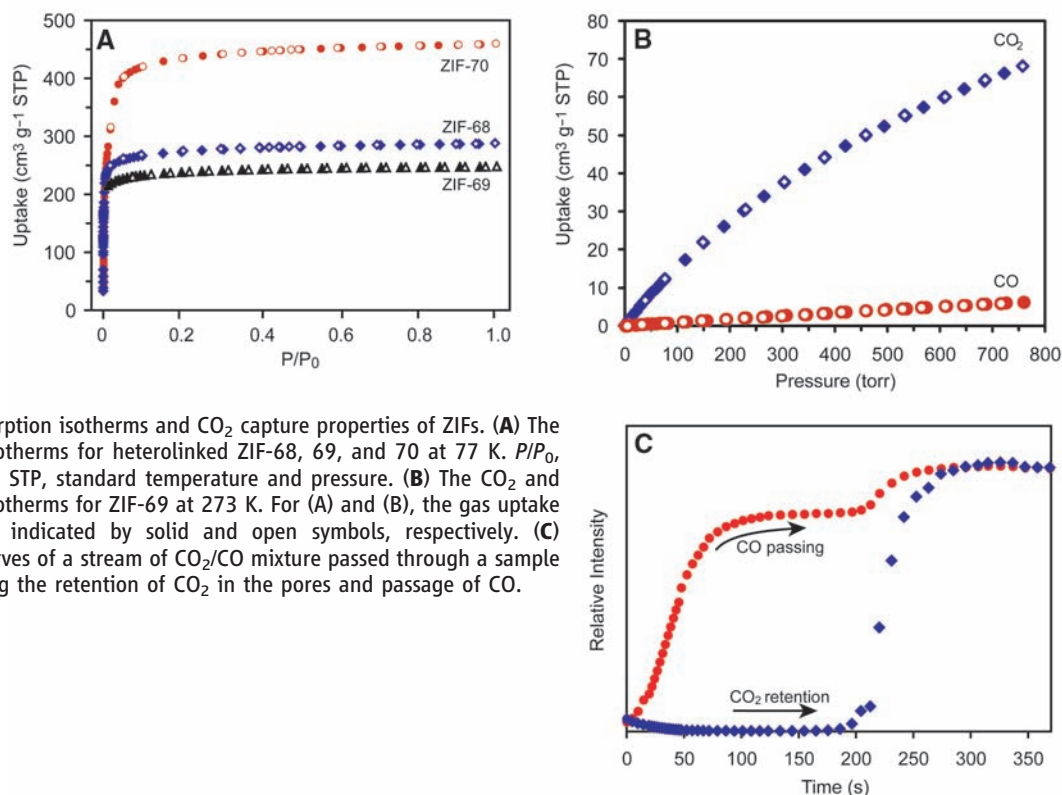


Fig. 2. Gas adsorption isotherms and CO₂ capture properties of ZIFs. (A) The N₂ adsorption isotherms for heterolinked ZIF-68, 69, and 70 at 77 K. *P/P*₀, relative pressure; STP, standard temperature and pressure. (B) The CO₂ and CO adsorption isotherms for ZIF-69 at 273 K. For (A) and (B), the gas uptake and release are indicated by solid and open symbols, respectively. (C) Breakthrough curves of a stream of CO₂/CO mixture passed through a sample of ZIF-68 showing the retention of CO₂ in the pores and passage of CO.

and a new structure (ZIF-60 to 77). Three (ZIF-68 to 70) have structures based on a zeolite topology (**gme**), which heretofore has not been achieved in metal-organic compounds, and five have tetrahedral topologies (**dia**, **cag**, **frl**, **lcs**, and **zni**) not occurring in zeolites. The nets of the structures are denoted by a bold lowercase three-letter symbol (*l8*) that is often the same as that of the corresponding zeolite net (Table 1). Furthermore, 10 structures (ZIF-60 to 62, 68 to 70, and 73 to 76) contain two chemically different imidazolate links (i.e., heterolinks). In the Cambridge Structural Database (version 5.28, January 2007), only 24 ZIF structures have been reported in the past 12 years; however, using the methodology described here, in 3 months, we optimized the reaction and identification conditions and produced crystals of ZIF-2 to 77 from the examination of only 9600 wells.

We analyze the complexity of the nets in terms of their natural tiling, which is a unique partition of space into tiles such that the set of edges and vertices of the tiles is the same as that of the net (*19*). A useful measure of structural complexity is the transitivity *pqrs*, which records that the tiling has *p* kinds of vertices, *q* kinds of edges, *r* kinds of faces, and *s* kinds of tiles. Of the 14 topologies recorded in Table 1 and shown in Fig. 1, all but one (**frl**) have just one kind of vertex (uninodal). Of the 176 recognized zeolite topologies, 21 are uninodal; we have found 9 of these in this study. Of the uninodal zeolite nets, only three (GIS, SOD, and ABW) have just one kind of tile (isohedral), and we have found two of them.

Of the five nonzeolite nets found and mentioned above, four are uninodal and three are isohedral. In contrast to the synthesis of zeolites, in ZIF chemistry, we are selecting the simpler nets in the synthesis. Indeed, the most complex zeolite net has transitivity 24 27 41 19 (*20*), which suggests that there is vast potential for the use of this high-throughput method in accessing ZIFs with structures based on more complex zeolites. The only binodal net (**frl**) found is of interest because it is simply related to the net (**sra**) of the missing isohedral zeolite net ABW, as detailed elsewhere (*21*). The topology (**lcs**) of ZIF-72 is also of interest because it is that of an invariant lattice complex (symbol *S*), but, despite its simplicity, it has not been previously reported in any tetrahedral structure.

We tabulate the density of the ZIFs using the traditional zeolite measure of the number of tetrahedral vertices per unit volume (*T/V*) (Table 1). The density (*T/V*) of an IM analog (i.e., ZIF) is

typically one-eighth that of a silicate zeolite because, in an IM framework containing zinc(II), the Zn...Zn distance is ~6.0 Å, whereas the corresponding Si...Si distance in a silicate is ~3.0 Å. For the structures reported here, *T/V* is in the range 2.0 to 4.6 nm⁻³; whereas the density for oxide zeolites is 12 to 20 nm⁻³. This difference indicates that ZIF frameworks are more open and more amenable to functionalization of their pores.

The existence of two different types of IMs with a side chain (especially an NO₂ or a CH₃ group) or an aromatic ring on the link makes the pore heterogeneously functionalized across the series (Fig. 1). Furthermore, the diameter of the largest sphere that will pass through that pore (*d_a*) ranges from as low as 0.7 Å to as high as 13.1 Å, whereas the diameter of the largest sphere that will fit into the cavities (*d_p*) varies from 0.7 to 15.9 Å. With the exception of ZIF-69, 71, 72, and 77, H atoms are nearest to the center of the cavity, and we have used a van der Waals radius of 1.2 Å for H in determining the appropriate sphere size. For ZIF-69, 71, 72, and 77, where the atoms nearest to the center of the cages are either Cl (69, 71, and 72) or O (77), van der Waals radii of 1.8 Å (Cl) and 1.5 Å (O) were used. The values of *d_a* and *d_p* provide a lower limit to the cage volume because, in some cases, the cages are ellipsoidal. The number of vertices of the largest cage in each structure ranges from 10 (**dia**) to 48 (**lta**). The cage face symbol (in which [...^{*m*}...]) signifies that the cage has *m* faces that are *n* rings) and the transivities of the nets are given in Table 1.

In all of the ZIFs, a Zn or Co atom is connected to four IM or substituted IM linkers to create a corresponding tetrahedron (Fig. 1 and SOM text S2). The tetrahedra are linked by corner-sharing into different three-dimensional zeolitic frameworks. However, these ZIFs differ in the nature of the functional groups decorating the pores and in the metrics of their pore structure (Table 1). Across the series, the metrics are systematically varied in increments of less than 1 Å; such tunability is unusual and potentially useful in gas adsorption and separation. We first needed to show for the ZIFs of interest that the microscale synthesis and the reaction conditions used for their discovery in the high-throughput instrument could be translated into multigram-scale bulk synthesis. For seven chosen ZIFs of heterolinks (ZIF-60, 61, 68 to 70, 74, and 76), we found that the microsynthesis conditions are scalable to 10-g scale and pure ZIF materials can thus be obtained (SOM text S1).

We targeted ZIF-68, 69, and 70 for adsorption studies because they all have the same topology (**gme**) and large pores (7.2, 10.2, and 15.9 Å in diameter for ZIF-69, 68, and 70, respectively) connected through tunable apertures (4.4, 7.5, and 13.1 Å). These ZIFs are permanently porous metal-organic frameworks in which the pore walls contain heterogeneous link functionality. We first examined the structural, thermal, and chemical stability, as well as the porosity, of these ZIFs. Thermal gravimetric analysis (TGA) was performed on the as-synthesized, solvent-exchanged, and activated ZIF products of ZIF-68 to 70, which revealed a thermal stability range of up to 390°C. Specifically, the TGA trace for these ZIFs showed a gradual weight-loss step between 25° and 168°C. A plateau between 150° and 390°C indicates that the evacuated framework has high thermal stability (SOM text S3). The evacuated frameworks of ZIF-68 to 70 thus produced have PXRD patterns that are coincident with the corresponding patterns simulated from single-crystal XRD structures (SOM text S3), which indicates that heterolinked ZIF frameworks have high structural and thermal stability. Examination of their chemical stability was performed by heating the samples in boiling benzene, methanol, and water for 7 days: conditions that reflect potential extreme industrial requirements. Notably, all of the ZIFs retained their structures under these conditions, as evidenced by the sharp, unshifted diffraction lines in their PXRD patterns (SOM text S4).

The permanent porosity of these ZIFs was also demonstrated by N₂ adsorption measurements (*8*) (SOM text S5), which showed that they exhibit type I adsorption isotherm behavior typical of materials of permanent porosity (Fig. 2A). The Langmuir surface areas were 1220, 1070, and 1970 m² g⁻¹ for ZIF-68, 69, and 70, respectively; these surface areas are more than double those of the most porous zeolites (*22*) and significantly higher than those of other reported ZIFs (*8, 9*).

The exceptional stability and metric attributes of these ZIFs led us to evaluate their behavior for a particularly difficult gas separation: CO₂ from CO. The adsorption isotherms for all three ZIFs show a disproportionately high affinity and capacity for CO₂ (SOM text S5), with ZIF-69 outperforming ZIF-68 and ZIF-70, as well as the state-of-the-art material BPL carbon (*23*) (Table 2 and Fig. 2B). Adsorption is completely reversible, and we calculate that 1 liter of ZIF-69 can store 82.6 liters (162 g) of CO₂ at 273 K. The selectivity is further supported by preliminary breakthrough experiments, which show complete retention of CO₂ and passage of CO through the pores of ZIF-68, 69, and 70 when they are exposed to streams containing a binary mixture of CO₂/CO (50:50 v/v) at room temperature (Fig. 2C and SOM text S5). In comparison

Table 2. Comparison of gas separation selectivity of ZIFs and BPL carbon (SOM text S5).

Material	Gas pairs	ZIFs selectivity	BPL carbon selectivity (23)	Ratio ZIFs/BPL carbon
ZIF-68	CO ₂ /CO	19.2	7.5	2.6
ZIF-69	CO ₂ /CO	20.9	7.5	2.8
ZIF-70	CO ₂ /CO	37.8	7.5	5.0

with that of BPL carbon, ZIFs have higher selectivity (Table 2). In terms of storage capacity and selectivity to CO₂, ZIF-69 and 70 outperform BPL carbon and all the other ZIFs that we have examined.

References and Notes

- D. E. Akporiaye, I. M. Dahl, A. Karlsson, R. Wendelbo, *Angew. Chem. Int. Ed.* **37**, 609 (1998).
- J. Klein, C. W. Lehmann, H. W. Schmidt, W. F. Maier, *Angew. Chem. Int. Ed.* **37**, 3369 (1998).
- K. Choi, D. Gardner, N. Hilbrandt, T. Bein, *Angew. Chem. Int. Ed.* **38**, 2891 (1999).
- R. Lai, B. S. Kang, G. R. Gavalas, *Angew. Chem. Int. Ed.* **40**, 408 (2001).
- M. Forster, N. Stock, A. K. Cheetham, *Angew. Chem. Int. Ed.* **44**, 7608 (2005).
- N. Stock, T. Bein, *Angew. Chem. Int. Ed.* **43**, 749 (2004).
- A. Corma, M. J. Díaz-Cabanas, J. L. Jordá, C. Martínez, M. Moliner, *Nature* **443**, 842 (2006).
- K. S. Park *et al.*, *Proc. Natl. Acad. Sci. U.S.A.* **103**, 10186 (2006).
- H. Hayashi, A. P. Côté, H. Furukawa, M. O'Keeffe, O. M. Yaghi, *Nat. Mater.* **6**, 501 (2007).
- R. Lehnert, F. Seel, *Z. Anorg. Allg. Chem.* **464**, 187 (1980).
- S. J. Rettig, V. Sánchez, A. Storr, R. C. Thompson, J. Trotter, *J. Chem. Soc. Dalton Trans.* **2000**, 3931 (2000).
- Y. Liu, V. Ch. Kravtsov, R. Larsena, M. Eddaoudi, *Chem. Commun.* **2006**, 1488 (2006).
- J.-P. Zhang, X.-M. Chen, *Chem. Commun.* **2006**, 1689 (2006).
- Y.-Q. Tian *et al.*, *Chem. Eur. J.* **13**, 4146 (2007).
- C. Baerlocher, L. B. McCusker, Database of Zeolite Structures (www.iza-structure.org/databases).
- M. E. Davis, *Nature* **417**, 813 (2002).
- The isolation of the sample array is accomplished in parallel by sonication and transfer in a custom-designed shallow metal plate, which allows the presence of a small amount of solvent during the PXRD data collection. The samples were then analyzed by a Bruker D8 DISCOVER high-throughput PXRD instrument with a movable horizontal x-y stage for automated analysis and an image plate detector system. The data collection time was 3 to 6 min per sample. The PXRD patterns thus collected were compared against an in-house library of PXRD patterns of known ZIFs and other network-type materials.
- Reticular Chemistry Structure Resource (<http://rcsr.anu.edu.au>).
- O. Delgado-Friedrichs, M. O'Keeffe, O. M. Yaghi, *Acta Crystallogr. A* **59**, 22 (2003).
- V. A. Blatov, O. Delgado-Friedrichs, M. O'Keeffe, D. M. Proserpio, *Acta Crystallogr.* **A63**, 418 (2007).
- N. L. Rosi *et al.*, *J. Am. Chem. Soc.* **127**, 1504 (2005).
- F. Rouquerol, J. Rouquerol, K. Sing, *Adsorption by Powders and Porous Solids* (Academic Press, London, 1999).
- S. Sircar, T. C. Golden, M. B. Rao, *Carbon* **34**, 1 (1996).
- The work was supported by Badische Anilin und Soda Fabrik (BASF) Ludwigshafen for synthesis, the U.S. Department of Energy (DEFG0206ER15813) for adsorption and separations studies, and the U.S. Department of Defense (W911NF-061-0405) for equipment used for breakthrough experiments. Crystallographic data for the structures reported in this paper have been deposited with the Cambridge Crystallographic Data Centre under reference numbers CCDC 671067 to 671089. These data can be obtained free of charge via www.ccdc.cam.ac.uk/contents/retrieving.html (or from the Cambridge Crystallographic Data Centre, 12 Union Road, Cambridge CB2 1EZ, UK).

Supporting Online Material

www.sciencemag.org/cgi/content/full/319/5865/939/DC1
SOM Text S1 to S5
Figs. S1 to S86
Tables S1 to S23

2 November 2007; accepted 3 January 2008
10.1126/science.1152516

Rogue Mantle Helium and Neon

Francis Albarède

The canonical model of helium isotope geochemistry describes the lower mantle as undegassed, but this view conflicts with evidence of recycled material in the source of ocean island basalts. Because mantle helium is efficiently extracted by magmatic activity, it cannot remain in fertile mantle rocks for long periods of time. Here, I suggest that helium with high ³He/⁴He ratios, as well as neon rich in the solar component, diffused early in Earth's history from low-melting-point primordial material into residual refractory "reservoir" rocks, such as dunites. The difference in ³He/⁴He ratios of ocean-island and mid-ocean ridge basalts and the preservation of solar neon are ascribed to the reservoir rocks being stretched and tapped to different extents during melting.

Helium-4 is a radiogenic nuclide produced in Earth and other planetary bodies by the alpha decay of uranium and thorium. In contrast, most of the ³He present is a regular stable nuclide. The relative abundances of the two isotopes in oceanic basalts therefore reflect the evolution of the parent/daughter ratio (U+Th)/He. These three elements are strongly incompatible (i.e., excluded from the structure of the major silicate materials), but one of them (He) is markedly affected by outgassing. Helium preferentially partitions not only into any gas phase present, but also into liquid during melting (1). Contribution from primitive undegassed mantle gives basalts very low ⁴He/³He ratios. The canonical model holds that high ⁴He/³He ratios characterize high (U+Th)/He mantle sources, such as the mantle underneath mid-ocean ridges, which were degassed during successive melting events. If He is less incompatible than both Th and U, however, these

low ³He/⁴He regions could instead signal mantle that was depleted in incompatible elements upon melting (1, 2). However, the abundances of rare gases differ between these two models, being high for undegassed mantle and very low for residual mantle.

For historical reasons, He isotopic compositions are reported upside down as R/R_{atm}, where R denotes the ³He/⁴He ratio and the subscript signals the normalization to the atmospheric ratio. More than 30 years of observations have shown that mid-ocean ridge basalts (MORBs) are characterized by a narrow range of ³He/⁴He ratios clustering about 8 R_{atm}, whereas values in excess of 20 R_{atm} are found nearly exclusively in ocean-island basalts (OIBs) (3–6). These data support the idea that MORBs are derived from parts of Earth's mantle that are significantly more degassed than the source of OIBs (5, 7, 8). If pushed to the extreme, the assertion that OIBs are tapping a deep, largely undegassed part of the mantle implies that the lower mantle is pristine and that mantle convection takes place as separate layers (9, 10).

This canonical view, however, conflicts with several critical observations on OIBs. Nearly every isotopic system involving lithophile elements—notably ⁸⁷Rb-⁸⁷Sr, ¹⁴⁷Sm-¹⁴³Nd, ¹⁷⁶Lu-¹⁷⁶Hf, and ¹⁸⁷Re-¹⁸⁷Os—indicates that the mantle source of MORB and OIB is de-

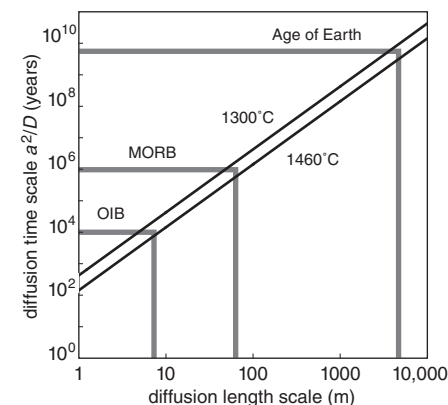


Fig. 1. Relationship between the time and length scales of diffusion in olivine, using the data of Shuster *et al.* (20) at two different temperatures. The two isotopes of He have comparable diffusion rates. At a temperature of 1460°C, He and Ne have the same diffusivity in quartz, which suggests that He and Ne diffusivity at mantle temperatures in mantle minerals may not be very different. The set of values labeled "Age of Earth" show that over the geological ages, He and Ne may have moved by diffusion over distances in excess of several kilometers. Assuming that melting takes place in the uppermost 100 km and an upwelling velocity of 10 m year⁻¹ beneath OIBs and 10 cm year⁻¹ beneath MORBs gives time scales for diffusion; the corresponding distances of diffusion relevant to melt extraction for MORB and OIB can be read from the curve (see text).